US 20250257648A1

(19) **United States**

(12) **Patent Application Publication** (10) **Pub. No.: US 2025/0257648 A1**

Hsu et al. (43) **Pub. Date: Aug. 14, 2025**

(54) **CEMENT EVALUATION THROUGH DUAL-STRING PIPES**

(71) Applicant: **Schlumberger Technology Corporation**, Sugar Land, TX (US)

(72) Inventors: **Kai Hsu**, Sugar Land, TX (US); **Toshihiro Kinoshita**, Sugar Land, TX (US); **Hiroaki Yamamoto**, Sugar Land, TX (US)

(21) Appl. No.: **19/047,798**

(22) Filed: **Feb. 7, 2025**

Related U.S. Application Data

(60) Provisional application No. 63/551,913, filed on Feb. 9, 2024.

Publication Classification

(51) **Int. Cl.**
E21B 47/005 (2012.01)

(52) **U.S. Cl.**
CPC ***E21B 47/005*** (2020.05); *E21B 2200/20* (2020.05)

(57) **ABSTRACT**

A method for cement evaluation through dual-string pipes comprising the steps of: i) acquiring waveforms data using a cement bond logging tool; ii) processing the acquired waveforms data to eliminate one or more potential DC offsets; iii) selecting a first receiver to further process the processed acquired waveforms data in a common-receiver domain; iv) performing in-situ calibration using the processed acquired waveforms data from the common-receiver domain to identify free-pipe and wall-bonded waveforms; v) calculating normalized amplitudes from monopole waveforms and azimuthal waveforms obtained from the free-pipe and wall-bonded waveforms to determine bond index and generate cement map; and vi) calculating statistical averages and variances using the calculated normalized amplitude to generate a final presentation.

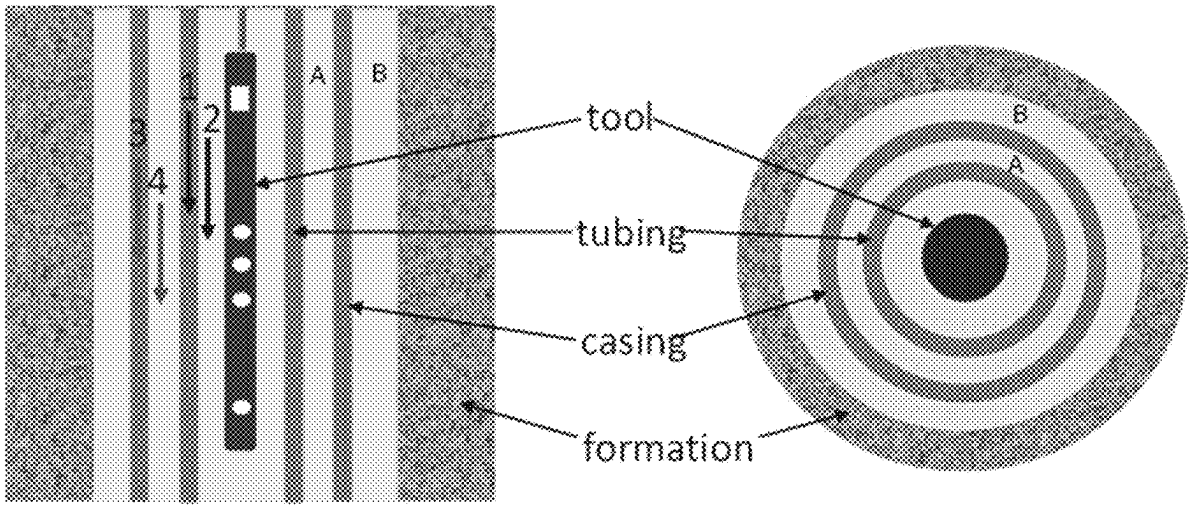

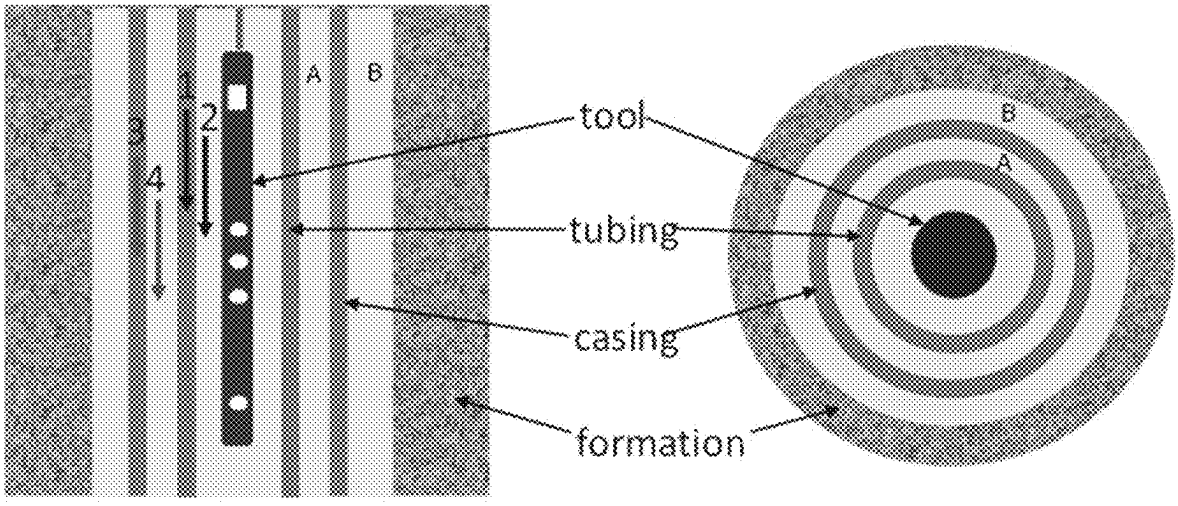

Figure 1

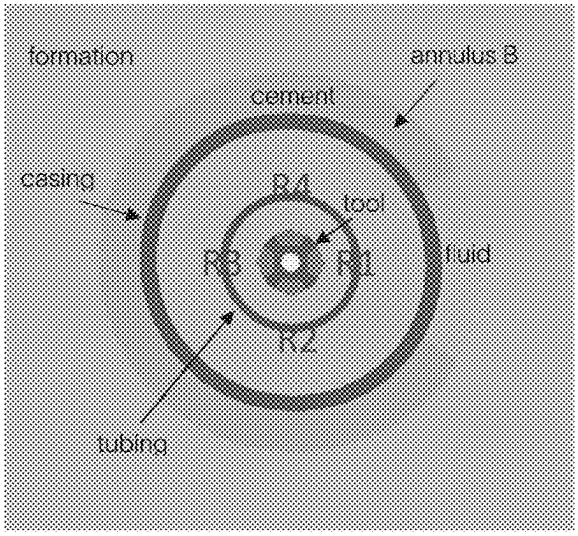

Figure 2

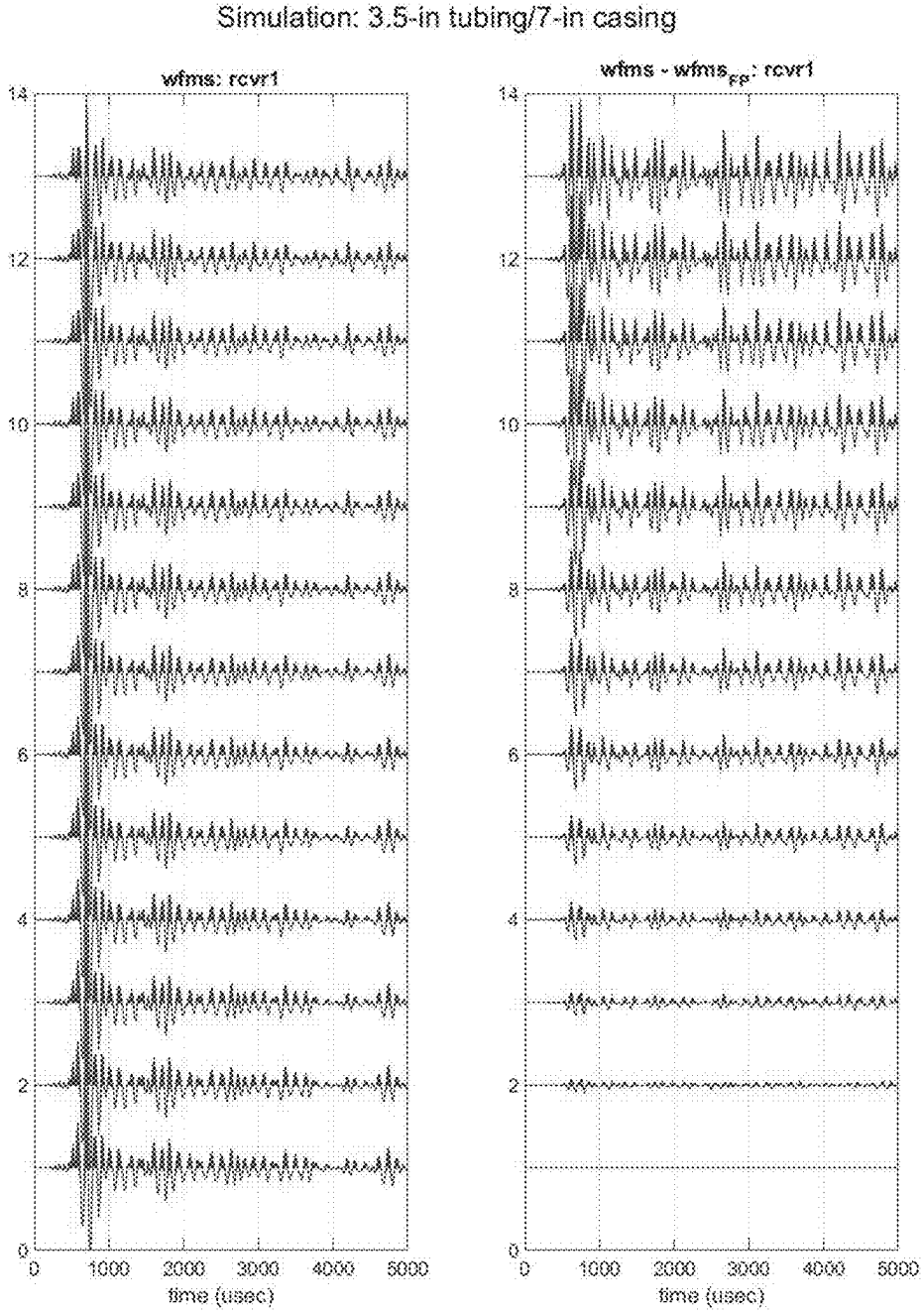
Simulation: 3.5-in tubing/7-in casing
wfms: rcvr1
wfms - wfms$_{FF}$: rcvr1
14
12
10
8
6
4
2
0
0
1000
2000
3000
4000
5000
time (usec)

Figure 3

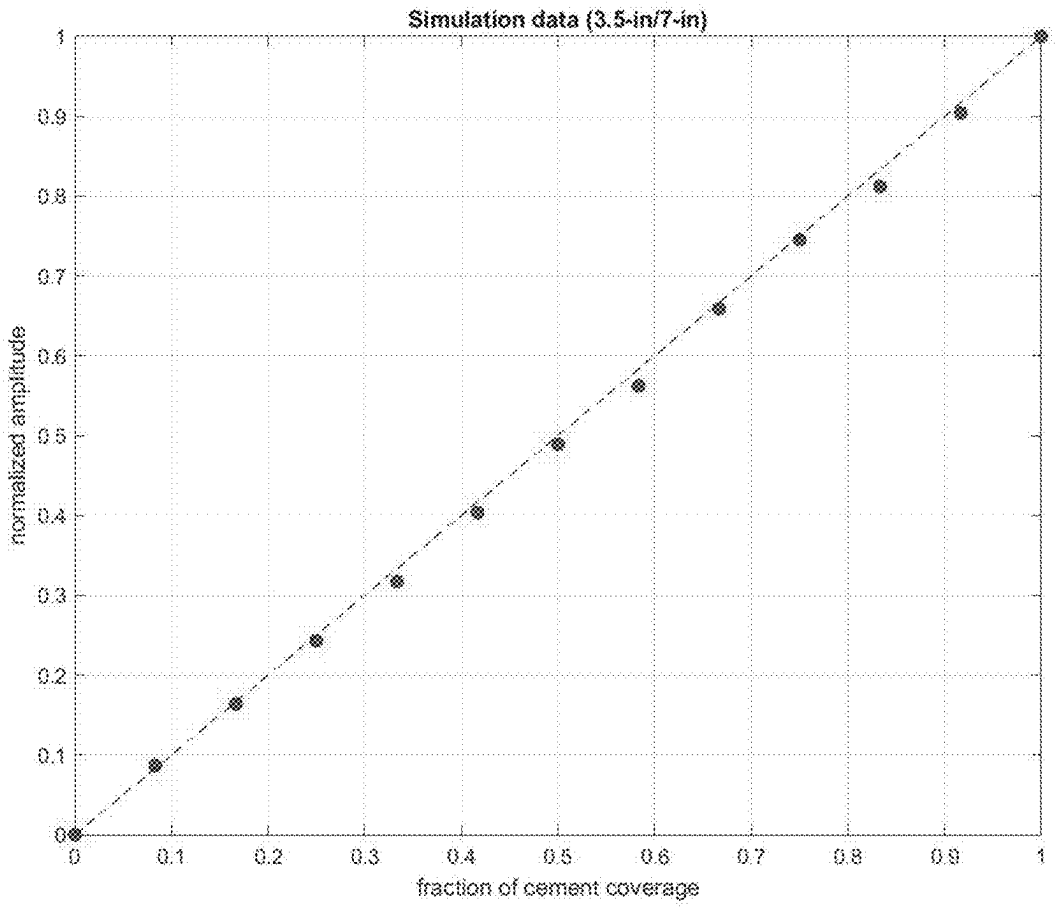
Simulation data (3.5-in/7-in)
normalized amplitude
fraction of cement coverage
0
0.1
0.2
0.3
0.4
0.5
0.6
0.7
0.8
0.9
1

Figure 4

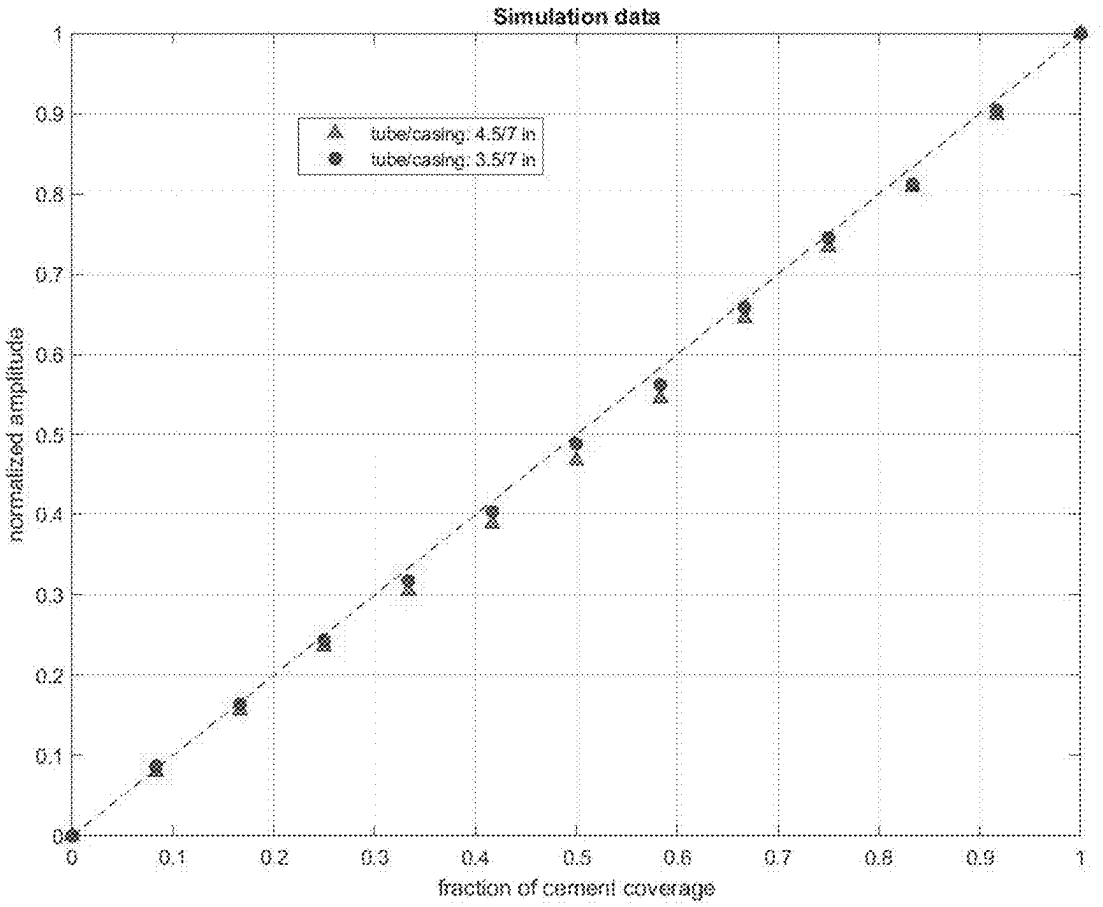
Simulation data
tube/casing: 4.5/7 in
tube/casing: 3.5/7 in
normalized amplitude
fraction of cement coverage
0
0.1
0.2
0.3
0.4
0.5
0.6
0.7
0.8
0.9
1

Figure 5

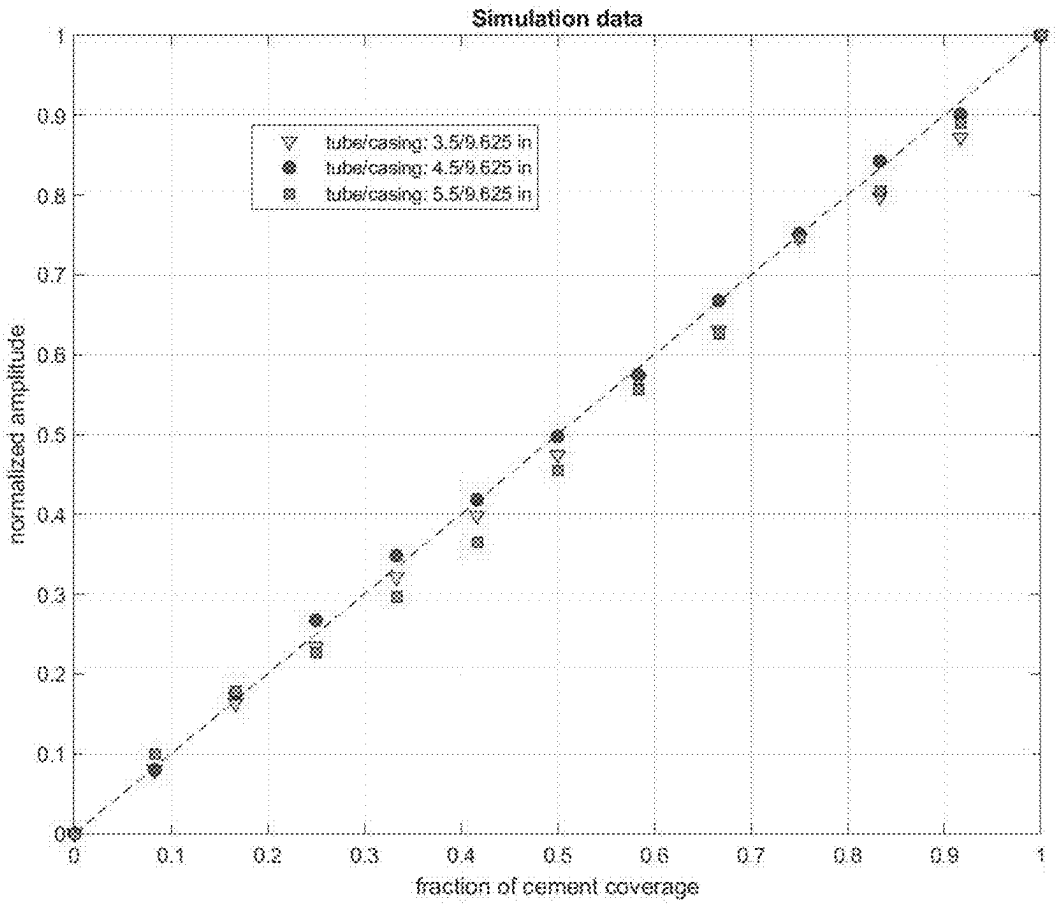
Simulation data
tube/casing: 3.5/9.625 in
tube/casing: 4.5/9.625 in
tube/casing: 5.5/9.625 in
normalized amplitude
fraction of cement coverage
0
0.1
0.2
0.3
0.4
0.5
0.6
0.7
0.8
0.9
1

Figure 6

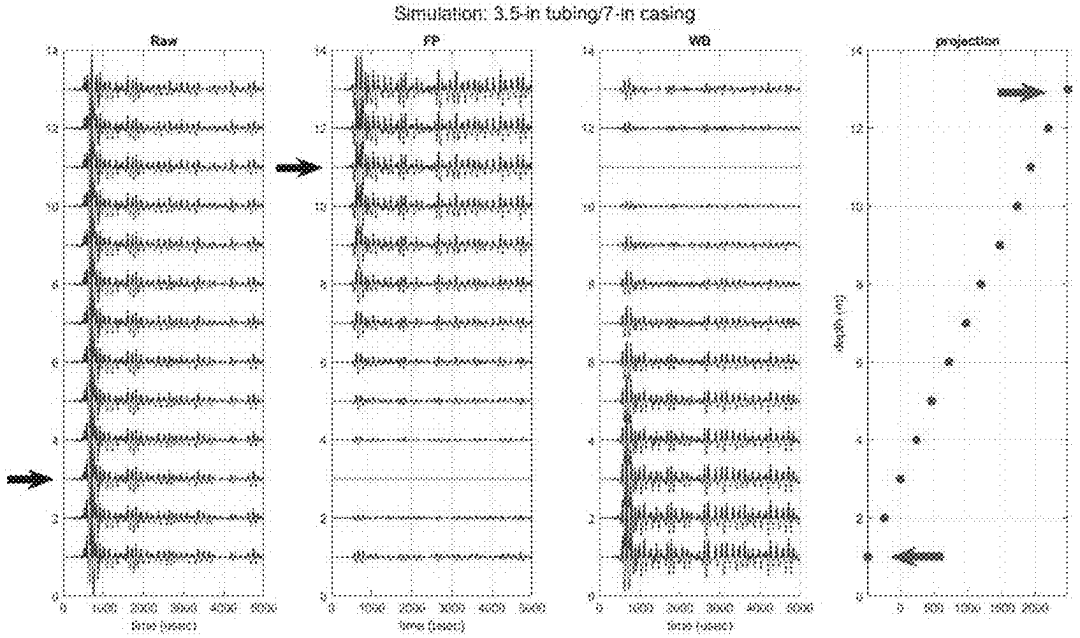

Figure 7

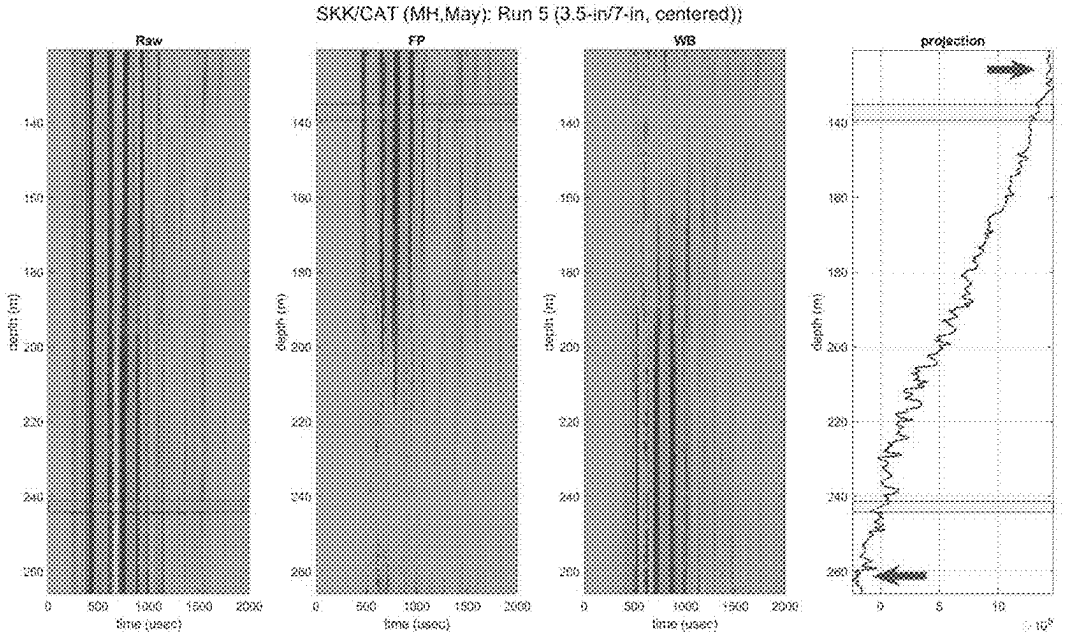

Figure 8

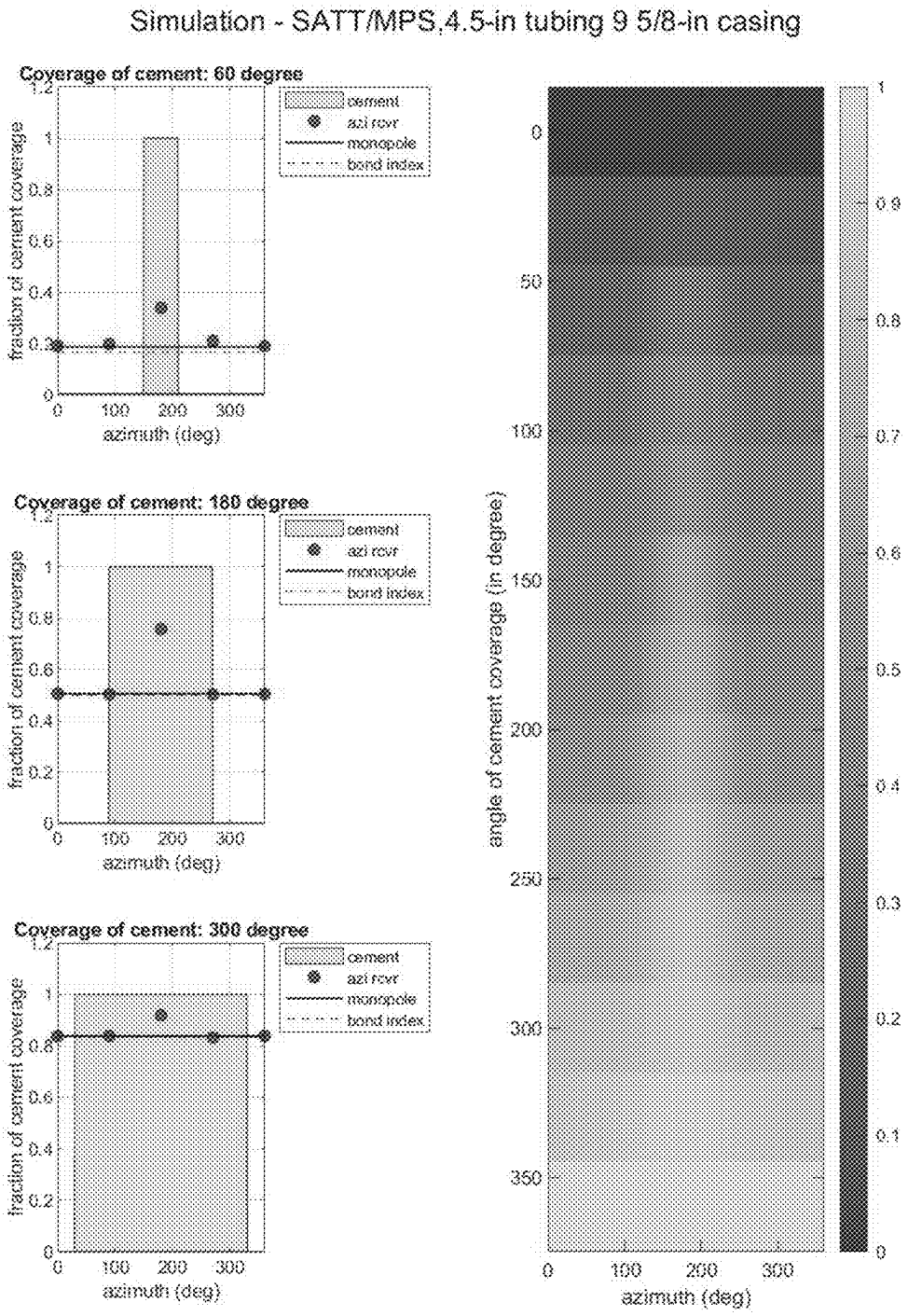
Simulation - SATT/MPS,4.5-in tubing 9 5/8-in casing
Coverage of cement: 60 degree
Coverage of cement: 180 degree
Coverage of cement: 300 degree
cement
azi rcvr
monopole
bond index
fraction of cement coverage
azimuth (deg)
angle of cement coverage (in degree)

Figure 9

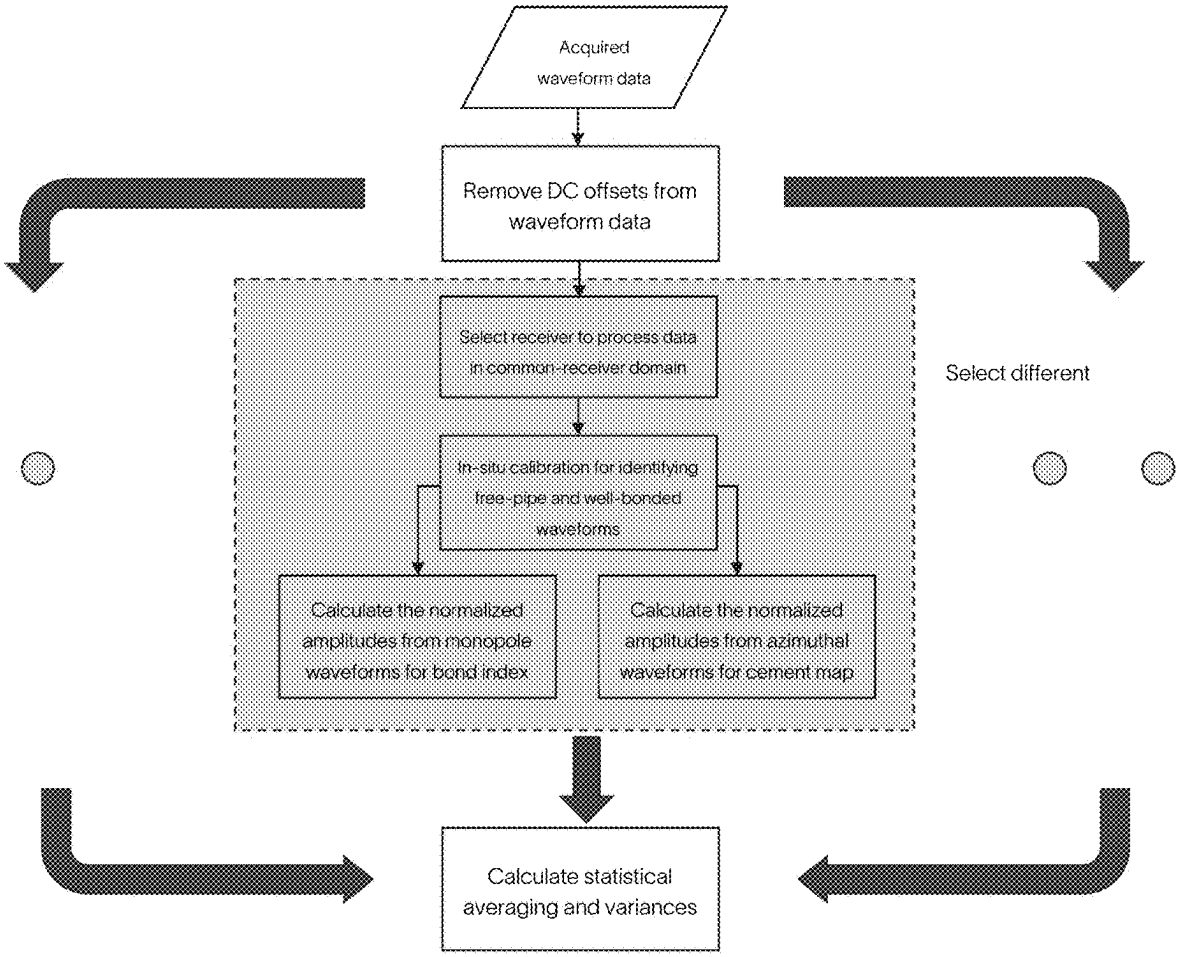
Acquired waveform data
Remove DC offsets from waveform data
Select receiver to process data in common-receiver domain
In-situ calibration for identifying free-pipe and well-bonded waveforms
Calculate the normalized amplitudes from monopole waveforms for bond index
Calculate the normalized amplitudes from azimuthal waveforms for cement map
Select different
Calculate statistical averaging and variances

Figure 10

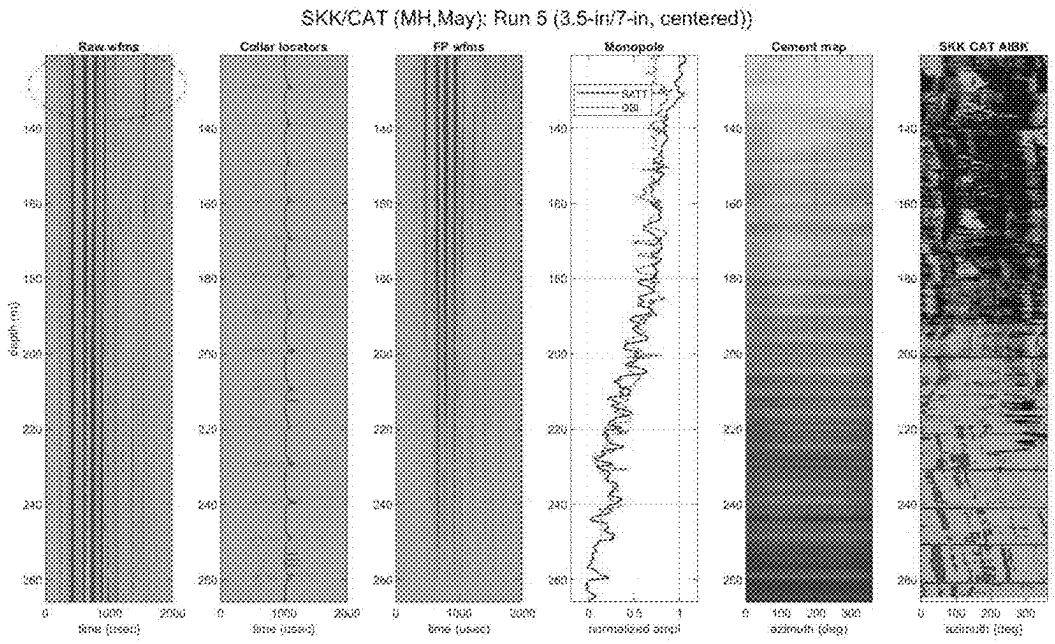

Figure 11

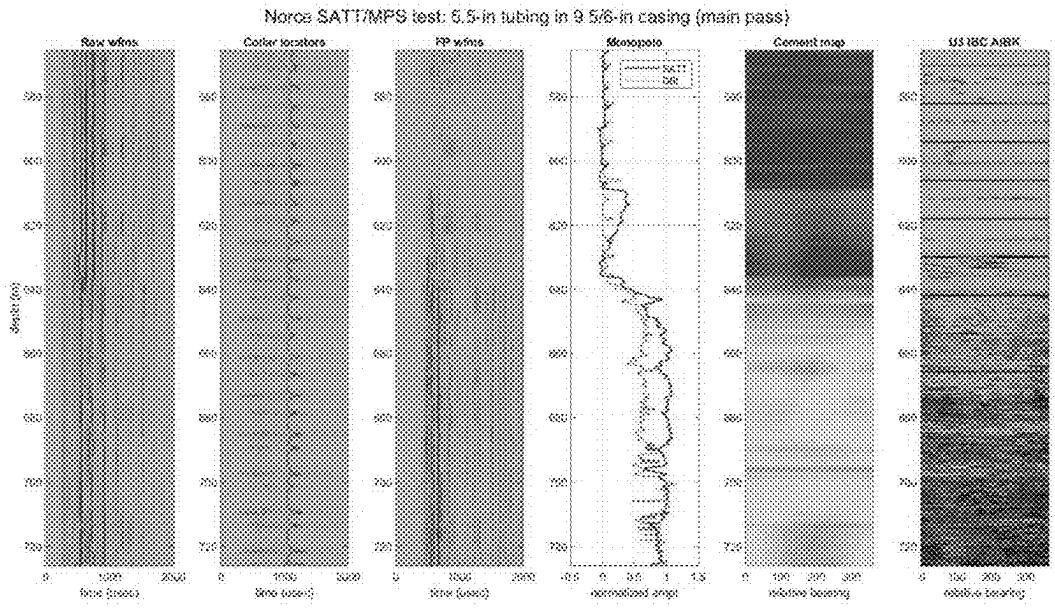

Figure 12

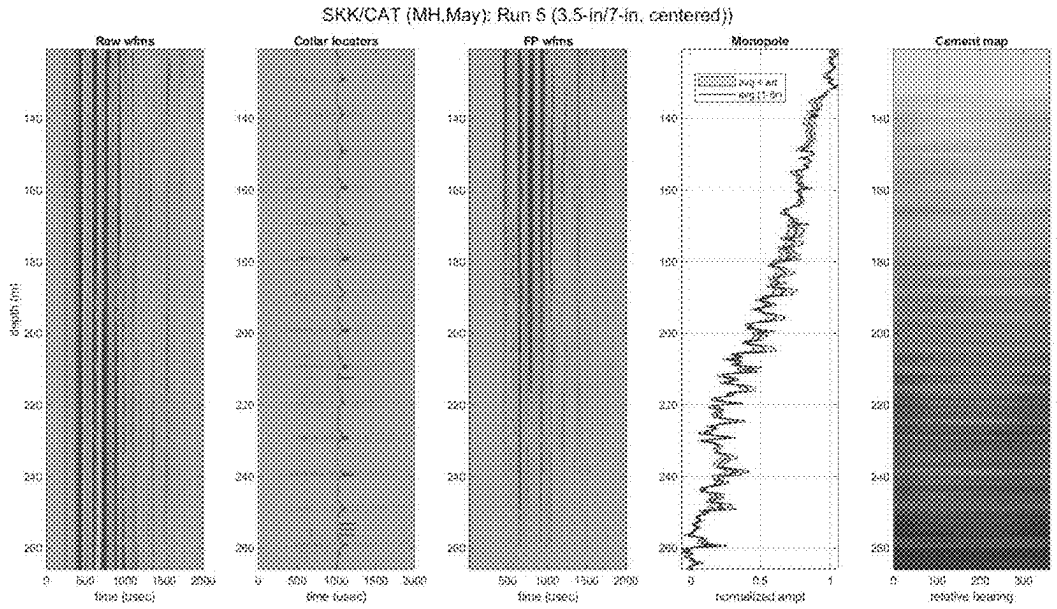
SKK/CAT (MH,May): Run 5 (3.5-in/7-in, centered))
Raw wfms
Collar locators
FP wfms
Monopole
Cement map
depth (m)
time (msec)
normalized ampl
relative bearing

Figure 13

CEMENT EVALUATION THROUGH DUAL-STRING PIPES

BACKGROUND

[0001] During the life cycle of a well, at a point when the well is no longer producing or not profitable anymore, this signifies the end of the well's lifetime. Therefore, oil companies will consider plugging the said well and temporarily stop production for a few months to years, or in certain situations, total abandonment of said wells. In most areas, the plugging and abandonment of such wells are regulated by a national agency to ensure there are no leaks to the surface, and that no formation fluid migration can occur even after many years of abandonment. All this is to make sure that there are no detrimental effects on the environment.

[0002] Depending on the condition and location of the well, plugging and abandonment (P&A) operations can differ and may be quite time-consuming as well as costly. For example, older wells often suffer from annular leaks or a loss of casing integrity that can further complicate the P&A operations, as these cases often require the operator to cut and pull tubulars or section mill casing in order to gain access to the leaking interval and seal it off. Moreover, in some situations, the well may be located offshore and may be costlier during P&A operations.

[0003] During a P&A operation, assessment of the cement sheath behind the casing is crucial for decommissioning oil and gas wells after extended periods of production. However, conventional evaluation methods primarily rely on acoustic logging measurements, which necessitate unimpeded access to the outer casing for traditional cement bond logging. This often requires the costly and time-consuming removal of production tubing or milling of the inner casing.

[0004] Therefore, there is a need for a method or system to assess the integrity and isolation of cement in wells with multi-string casings intact which can significantly reduce operational time and costs, while simplifying the conventional P&A operations and minimizing the carbon footprint associated with rig mobilization, tubing cutting, or milling.

BRIEF DESCRIPTION OF THE DRAWINGS

[0005] The present disclosure is best understood from the following detailed description when read with the accompanying figures. It is emphasized that, in accordance with the standard practice in the industry, various features are not drawn to scale. In fact, the dimensions of the various features may be arbitrarily increased or reduced for clarity of discussion.

[0006] FIG. **1** is a schematic of a logging scenario used to evaluate the cement sheath in the P&A operation without removing the production or inner tubing, according to one or more examples of the disclosure.

[0007] FIG. **2** is a cross-section of the simulation for the scenarios of FIG. **1**, according to one or more examples of the disclosure.

[0008] FIG. **3** is an array of thirteen waveforms from receiver 1, representing the progressive increase in cement coverage from the bottom to the top on the left panel, and corresponding residual waveforms after subtracting the free-pipe waveform on the right panel, for the case with a tubing OD of 3.5 inches and a casing OD of 7 inches, according to one or more examples of the disclosure.

[0009] FIG. **4** is a graph depicting the normalized amplitudes, as calculated using Equation (2), are plotted against the corresponding fraction of cement coverages for thirteen cases shown in FIG. **3**, according to one or more examples of the disclosure.

[0010] FIG. **5** is a graph depicting the calculated normalized amplitudes are plotted against the corresponding fraction of cement coverage for two tubing sizes (i.e., 3.5-inch and 4.5-inch) in the 7-inch casing, according to one or more examples of the disclosure.

[0011] FIG. **6** is a graph depicting the calculated normalized amplitudes are plotted against the fraction of cement coverage for the three tubing sizes (i.e., 3.5-inch, 4.5-inch, and 5.5-inch) in the 9⅝-inch casing, according to one or more examples of the disclosure.

[0012] FIG. **7** depicts the sequence of steps for selecting the free-pipe and well-bonded waveforms using the example shown in FIG. **3**, according to one or more examples of the disclosure.

[0013] FIG. **8** depicts the sequence of steps for selecting the free-pipe and well-bonded waveforms for the field data acquired from the SKK/CAT well using a CETT (Cement Evaluation Through Tubing) acoustic logging tool, according to one or more examples of the disclosure.

[0014] FIG. **9** depicts the results obtained from analyzing the azimuthal waveforms using a simulated scenario involving a 4.5-inch tubing and a 9⅝-inch casing The left side displays three snapshots whereas the right panel shows the interpolated cement image for thirteen cases, according to one or more examples of the disclosure.

[0015] FIG. **10** is a flowchart depicting a method for cement evaluation through dual-string pipes, according to one or more examples of the disclosure.

[0016] FIG. **11** depicts a suite of plots derived from a first field example involved running a 3.5-inch tubing with SATT in the 7-inch SKK CAT well, according to one or more examples of the disclosure.

[0017] FIG. **12** depicts a suite of plots derived from a second field example involved running SATT with the deployment of 5.5-inch tubing within the 9⅝-inch casing in the Norce U3 test well operated by Equinor in North Sea, according to one or more examples of the disclosure.

[0018] FIG. **13** depicts a third field example utilizing the SKK CAT well data depicted in FIG. **11** for demonstrating the combination of the computed results from multiple receivers, according to one or more examples of the disclosure.

DETAILED DESCRIPTION

[0019] Illustrative examples of the subject matter claimed below will now be disclosed. In the interest of clarity, not all features of an actual implementation are described in this specification. It will be appreciated that in the development of any such actual implementation, numerous implementation-specific decisions may be made to achieve the developers' specific goals, such as compliance with system-related and business-related constraints, which will vary from one implementation to another. Moreover, it will be appreciated that such a development effort, even if complex and time-consuming, would be a routine undertaking for those of ordinary skill in the art having the benefit of this disclosure.

[0020] Further, as used herein, the article "a" is intended to have its ordinary meaning in the patent arts, namely "one

or more." Herein, the term "about" when applied to a value generally means within the tolerance range of the equipment used to produce the value, or in some examples, means plus or minus 10%, or plus or minus 5%, or plus or minus 1%, unless otherwise expressly specified. Further, herein the term "substantially" as used herein means a majority, or almost all, or all, or an amount with a range of about 51% to about 100%, for example. Moreover, examples herein are intended to be illustrative only and are presented for discussion purposes and not by way of limitation.

[0021] The assessment of the cement sheath behind the casing is crucial in plug and abandonment (P&A) operations for decommissioning oil and gas wells after extended periods of production. However, conventional evaluation methods primarily rely on acoustic logging measurements, which necessitate unimpeded access to the outer casing for traditional cement bond logging. This often requires the costly and time-consuming removal of production tubing or milling of the inner casing. To address this challenge, the present invention is able to assess the integrity and isolation of cement in wells with multi-string casings intact, thus eliminating the need for removing the production or inner casing. Such an approach can significantly reduce operational time and costs, while simplifying the conventional P&A process and minimizing the carbon footprint associated with rig mobilization, tubing cutting, or milling.

[0022] A logging scenario is depicted in FIG. **1**, wherein the configuration involves two tubulars, with annulus A positioned between the tubing and the outer casing, and annulus B situated between the outer casing and the formation. This logging scenario offers a means to evaluate the cement sheath in the P&A operation without requiring the removal of the production or inner tubing, where an acoustics logging tool (with a transmitter and an array of receivers), is utilized for this purpose.

[0023] To-date, the conventional cement bond logging tool (CBL) utilizes monopole waveform data acquired through acoustic logging tools. Within the recorded waveforms, the complex wavefield can be divided into at least four propagation wave components, as indicated in FIG. **1**: 1) Extensional wave in the tubing, 2) Stoneley wave within the tubing, 3) extensional wave in the outer casing, and 4) Stoneley wave in annulus A. Depending on the bonding conditions in annulus B, the recorded waveforms may also encompass additional propagation wave components. The dominant events among these wave components are the Stoneley waves in categories 2 and 4, which propagate at slightly different speeds due to the different inner diameters of the tubing and casing. The first arrival on the waveforms corresponds to the extensional wave in the tubing. However, this wave is not sensitive to the filling conditions of cement/fluids in annulus B and, thus, cannot be employed to assess these conditions, as is typically done in conventional cement bond logging. Although the extensional wave in the outer casing (i.e., category 3) has the potential to convey information about the cement/fluid conditions, it is relatively weak and often overshadowed and obscured by other wave components.

[0024] In order to solve the above problems, the present invention observed a strong correlation between the amplitudes of these residual waveforms and the cement/fluid conditions (specifically, the bond index) obtained without removing the production tubing or inner casing. Alternatively, a different reference state can be established by finding the recorded waveforms in a well-bonded pipe, where annulus B is 100% filled with cement.

[0025] For the present invention, a model to validate the observed phenomenon through numerical simulations of wave propagation in dual-string casing situations in developed based on the simulation scenario presented in FIG. **1**. FIG. **2** shows the cross-section of the simulation, featuring an acoustic logging tool positioned at the center of the tubing, which itself is centered within the casing. The logging tool incorporates four azimuthal receiving elements (referred to as R1, R2, R3, and R4) for each station. In totality, there are 12 axial stations (aka 12 receivers) distributed at regular spacing of 4 inches and a monopole transmitter situated at 2 feet away from the nearest station. Moreover, behind the casing, there exists a fluid channel within annulus B, positioned in such a way that its center aligns with the receiving element R1. The remaining section of annulus B is filled with cement, forming a complete bond with the casing.

[0026] To explore various scenarios, thirteen cases of waveform simulations are conducted, ranging with the angle of channel aperture from 0° (well-bonded case) to 360° (free-pipe case), with increments of 30°. For each case, an array of waveforms is generated at twelve stations by firing the monopole transmitter. At each station, four azimuthal waveforms are recorded by the respective receiving elements, and the monopole waveform at each station is obtained by summing the four azimuthal waveforms. This memorandum refers to the waveform recorded by a receiver as the monopole waveform corresponding to its respective station. The waveform at receiver 1, for example, means the monopole waveform recorded at station 1.

[0027] To demonstrate the proposed method of the present invention, an example involving a tubing inner diameter (ID) of 3.5 inches and a casing OD of 7 inches, both having nominal thicknesses is used, and the approach involves subtracting the free-pipe waveform from the raw waveforms. This is done in the common-receiver domain, i.e. the waveforms from the same receiver over different scenarios and in the case of field data, over various depths. FIG. **3** showcases the waveforms at the 1st receiver station (receiver 1) for all thirteen cases, both before and after the subtraction. The y-axis index, denoted by "i," corresponds to the case number, also relating to the fraction of cement coverage (a), also known as the bond index, as

$$\alpha = \frac{(i-1)*30}{360} \tag{1}$$

[0028] Hence, FIG. **3** displays a series of thirteen waveforms from receiver 1, representing the progressive increase in cement coverage from the bottom to the top. The waveform labeled as index 1 corresponds to the free-pipe condition, while index 13 represents a well-bonded state. Note that the raw waveforms in the left panel appear almost identical, regardless the the changing cement coverage behind the casing. However, upon subtracting the free-pipe waveform, the residual waveforms showcased in the right panel exhibit noticeable variations in amplitude. These variations exhibit a strong correlation with the fraction of cement coverage. The correlation leads us to compute the normalized amplitude for further exploiting the strong correlation.

[0029] The free-pipe waveform is denoted as $wfm_{FP}(t)$, while the well-bonded waveform as wfm_{WB} (t), and the waveform with an unknown bond index α as $wfm_{\alpha}(t)$. The normalized amplitude is computed as

$$\text{normalized amplitude} = \frac{\underset{t\epsilon T,\ f\epsilon B}{\text{RMS}} \left(wfm_{\alpha}(t) - wfm_{FP}(t)\right)}{\underset{t\epsilon T,\ f\epsilon B}{\text{RMS}} \left(wfm_{WB}(t) - wfm_{FP}(t)\right)} \quad (2)$$

[0030] In this calculation, the numerator represents the root-mean-square (RMS) amplitude of the residual waveform, while the denominator corresponds to the root-mean-square (RMS) amplitude of the difference waveform between the well-bonded and free-pipe waveforms. Both the RMS amplitudes are computed within a specified time window T and frequency band B.

[0031] Meanwhile, FIG. **4** shows the normalized amplitudes derived from the waveforms, as calculated using Equation (2), against the corresponding fraction of cement coverages for thirteen cases shown in FIG. **3**. The results demonstrate a nearly linear relationship between the normalized amplitude and the fraction of cement coverage. Additionally, these findings suggest that the normalized amplitude can serve as an estimation for the fraction of cement coverage (i.e., bond index).

[0032] To further examine the effects of different tubing and casing sizes, additional cases were added into the investigation. Table 1 provides a study identifying potential candidates for P&A (plug and abandon) operations within the field, denoted by "x". Based on the information presented in the table, simulations were conducted, and the same analysis was performed for the other candidates denoted by "O".

TABLE 1

The tubing and casing combinations for P&A wells in field.

	3.5-in	4.5-in	5.5-in
7-in	X	○	
9⅝-in	○	○	○

[0033] FIG. **5** shows the crossplot between normalized amplitude and the corresponding fraction of cement coverage for two cases involving 7-inch casings. The results obtained from the 4.5-inch tubing case are superimposed on the findings obtained from the 3.5-inch tubing case, as depicted in FIG. **4**. Similar to the 3.5-inch tubing case, the results obtained from the 4.5-inch tubing case also demonstrate a strong linear relationship in relation to the fraction of cement coverage. Within the 9⅝-inch casing, three potential tubing sizes are identified: 3.5-inch, 4.5-inch, and 5.5-inch. Waveform simulations are performed for these three tubing sizes within the 9⅝-inch casing. The results of normalized amplitude versus the fraction of cement coverage are presented in FIG. **6**, following the same processing and analysis methodology as before. While the calculated normalized amplitudes do not strictly follow a linear relationship along the diagonal line for all three scenarios, a close linear approximation is observed.

[0034] Therefore, based on the results shown in FIGS. **4-6**, the following approximation model can be established as the foundation for further development.

$$wfm_{\alpha}(t) \approx (1-\alpha) * wfm_{FP}(t) + \alpha * wfm_{WB}(t) \quad (3)$$

FEATURES OF THE PRESENT INVENTION

[0035] The features of the prevent invention are further explained below in detail, which encompasses the algorithm used in the present invention, in-situ calibration of the present invention, bond index, and the creation of a cement map.

ALGORITHM OF THE PRESENT INVENTION

[0036] In one embodiment of the present invention, the algorithm is then further developed based on Equ. (3), and starts with subtracting the free-pipe waveform from the recorded waveforms with the unknown fraction of cement coverage a, which is equivalent to

$$wfm_{\alpha}(t) - wfm_{FP}(t) \approx \alpha * (wfm_{WB}(t) - wfm_{FP}(t)) \quad (4)$$

[0037] An estimate of a was proposed earlier using the root-mean-squares (RMS) approach, i.e.,

$$\alpha \approx \frac{\underset{t\epsilon T,\ f\epsilon B}{\text{RMS}} \left(wfm_{\alpha}(t) - wfm_{FP}(t)\right)}{\underset{t\epsilon T,\ f\epsilon B}{\text{RMS}} \left(wfm_{WB}(t) - wfm_{FP}(t)\right)} \quad (5)$$

[0038] The RMS approach proves effective in handling simulated data without noise. However, its performance degrades when applied to field data due to the presence of noise. Equ. (5) is unable to adequately filter out the noise during calculations. To address this limitation, a superior and robust approach is proposed, leveraging the minimum-mean-squares error (MMSE) criteria.

$$\min_{\alpha} \sum_{t\in T, f\in B} \left(wfm_{\alpha}(t) - wfm_{FP}(t) - \alpha * (wfm_{WB}(t) - wfm_{FP}(t))\right)^2 \quad (6)$$

[0039] It is important to note that in Equ. (6), the model is incorporated within the minimization criteria, allowing for the effective exclusion of noise that does not conform to the model (i.e., Equ. (4)).

In-Situ Calibration of the Present Invention

[0040] In one embodiment of the present invention, to estimate the fraction of cement coverage a using either the RMS approach (Equ. (3)) or the MMSE approach (Equ. (6)), it is necessary to have knowledge of the free-pipe waveform and the well-bonded waveform under the same dual-string conditions (i.e., same tubing and casing sizes) as the recorded waveforms with the unknown a. Both the free-pipe

waveform and the well-bonded waveform can be estimated from the recorded waveforms through an in-situ calibration procedure.

[0041] The algorithm is illustrated using the example depicted in FIG. **3**. The sequence of steps for selecting the free-pipe and well-bonded waveforms is presented in FIG. **7**. The algorithm starts with an initial guess of the free-pipe waveform, denoted as $\widehat{wfm_{FP}}$ t) with an unknown g, i.e.,

$$\widehat{wfm_{FP}}(t) \approx (1-\gamma)*wfm_{FP}(t)+\gamma*wfm_{WB}(t) \tag{7}$$

[0042] In the first panel, for example, the initial step involves selecting the free-pipe raw waveform of index 3 (indicated by an arrow). Moving to the second panel, the residual waveforms are displayed after subtracting the selected free-pipe raw waveform (i.e., $\widehat{wfm_{FP}}$ (t)) from the raw waveforms shown in the first panel. From these residual waveforms, the algorithm identifies a raw waveform with a significant residual waveform amplitude, indicating a better bonded raw waveform. In this particular example, the raw waveform of index 11 (highlighted by an arrow in the second panel) is chosen as the better bonded raw waveform. It is denoted as estimated ($\widehat{wfm_{WB}}$ (t), with an unknown b.

$$\widehat{wfm_{WB}}(t) \approx (1-\beta)*wfm_{FP}(t)+\beta*wfm_{WB}(t) \tag{8}$$

[0043] In the third panel, the residual waveforms are displayed after subtracting the estimated well-bonded raw waveform (i.e., $\widehat{wfm_{WB}}$ (t)) from the raw waveforms. The purpose of comparing the second and third panels side by side is to demonstrate the consistent amplitude trends observed in the corresponding residual waveforms.

[0044] Specifically, the residual waveforms obtained after subtracting the free-pipe waveform exhibit large amplitudes in the waveforms associated with better cement bonding conditions, while waveforms closer to the free-pipe conditions exhibit smaller amplitudes. Conversely, the residual waveforms obtained after subtracting the well-bonded waveform (shown in the third panel) demonstrate a consistent reverse trend. Waveforms with better cement bonding conditions exhibit smaller amplitudes, whereas waveforms closer to the free-pipe conditions display larger amplitudes. The consistent check is to ensure b>g.

[0045] Mathematically, the the residual waveforms in the second panel can be expressed as

$$wfm_a(t)-\widehat{wfm_{FP}}(t) \approx (\alpha-\gamma)*(wfm_{WB}(t)-wfm_{FP}(t)) \tag{9}$$

[0046] where wfm_a (t) are the raw waveforms with unknown a. Knowing the initial selection of $\widehat{wfm_{WB}}$ (t) and $\widehat{wfm_{WB}}$ (t), we can also compute the following difference

$$\widehat{wfm_{WB}}(t)-\widehat{wfm_{FP}}(t) \approx (\beta-\gamma)*(wfm_{WB}(t)-wfm_{FP}(t)) \tag{10}$$

[0047] The last stage of the algorithm involves projecting the residual waveforms from Equ. (9) onto the difference waveform defined in Equ. (10) over a specified time window (T) and frequency band (B). Mathematically, this projection, denoted as P(α), corresponds to the inner product between the two quantities, i.e.

$$P(\alpha) = (\alpha-\gamma)*(\beta-\gamma)*\sum_{t\in T, f\in B}(wfm_{WB}(t)-wfm_{FP}(t))^2 \tag{11}$$

[0048] In the last panel of FIG. **7**, the projection P(a) for the given example is displayed. The magnitude and polarity of P(a) are primarily determined by the first term (a-g) on the right-hand side of Equ. (11), as the last two terms are fixed and positive values. Consequently, the well-bonded raw waveform that yields the largest and often positive projection is considered the best candidate for the well-bonded waveform. Conversely, the free-pipe raw waveform that results in the smallest and often negative projection is identified as the best candidate for the free-pipe waveform.

[0049] Applying this criterion, the algorithm determines the raw waveform of index 1 as the free-pipe raw waveform and the raw waveform of index 13 as the well-bonded waveform. Both of them are highlighted by red arrows in the final panel of FIG. **7**.

[0050] To demonstrate the algorithm's effectiveness, the algorithm was applied to field data acquired from the SKK/CAT well using a CETT (Cement Evaluation Through Tubing) acoustic logging tool. The tool's configuration matched the setup described in the simulation. Specifically, it was deployed with a 3.5-inch tubing inside the 7-inch cased hole section, covering approximately 120 meters to 270 meters.

[0051] FIG. **8** illustrates the step-by-step process for identifying the free-pipe and well-bonded waveforms, following a similar approach as shown in FIG. **7**. However, instead of using a wiggle-trace plot for waveforms, they are displayed using a color Variable Density Log (VDL).

[0052] In the first panel of FIG. **8**, the raw waveforms from receiver 1 are displayed, highlighting an initial free pipe interval. It should be noted that for the field data, an appropriate free pipe interval may be selected to enable the use of a robust averaging scheme such as trimmed-mean or median filtering over the selected interval to obtain an initial estimate of the free-pipe waveform.

[0053] Moving to the second panel, the Variable Density Log (VDL) of the residual waveforms is displayed after subtracting the estimated free-pipe waveform from the raw waveforms shown in the first panel. Based on the residual waveforms in the second panel, a better bonded interval with significant residual amplitudes is selected to estimate a better bonded waveform. Once again, we can use the robust averaging scheme over the selected interval to obtain an estimate of a better bonded waveform.

[0054] The third panel showcases the VDL of the residual waveforms obtained by subtracting the estimated better bonded waveform from the raw waveforms shown in the first panel. As observed in the simulation data example (FIG. **6**), the residual waveform amplitudes in both the second and third panels consistently reveal a consistent inverse trend in the amplitudes of the residual waveforms.

[0055] The final panel of FIG. **8** presents the computed projections using Equation (11). Additionally, the display highlights two intervals (highlighted in yellow) that have been selected for the calculation of the free-pipe waveform and the well-bonded waveform. Based on the projections, it

is evident that the zone ranging from 260-265 m is the most suitable candidate for estimating the free-pipe waveform, while the zone from 130-135 m is identified as the best candidate for estimating the well-bonded waveform. These estimates align with our understanding of the CAT well cement bonding conditions.

[0056] As a final note, the in-situ calibration algorithm described herein has the ability to identify the most suitable candidates for the free-pipe and well-bonded waveforms from the available waveforms within the desired depth interval. If no free-pipe section is present, the algorithm should identify the closest waveform that resembles the free-pipe condition. The same principle applies to the identification of the well-bonded waveform.

Bond Index and the Creation of Cement Map

[0057] In the same embodiment of the present invention, as previously mentioned, the normalized amplitude of the monopole can be used to estimate the fraction of cement coverage, also known as the bond index. The monopole waveforms are obtained by combining the waveforms of azimuthal receivers at different levels. Since the waveforms captured by the azimuthal receivers contain valuable information about the distribution of cement around the hole, the potential of creating a cement map using these azimuthal waveforms was investigated.

[0058] For demonstration purposes, a simulated scenario involving a 4.5-inch tubing and a 9⅝-inch casing was utilized. The simulation example comprises a tool with 12 receivers positioned within the tubing. Each receiver is accompanied by four azimuthal receivers, evenly distributed around the tool with a 90-degree separation. Similar to previous simulations, thirteen cases were considered, varying the angle of the channel aperture from 0° (representing a well-bonded case) to 360° (representing a free-pipe case), with increments of 30°. The waveforms obtained from the azimuthal receivers are employed to calculate the azimuthal normalized amplitudes using the same methodology applied to the monopole waveforms.

[0059] In FIG. **9**, the results obtained from analyzing the azimuthal waveforms was observed at receiver 1. The left side displays three subplots showcasing snapshots of the estimated fraction of cement coverage as red dots, plotted against azimuthal angles. For comparison, the true cement coverage is depicted by a yellow band, the estimated fraction of cement coverage using monopole waveforms is represented by a black line, and the bond index based on the cement distribution is indicated by a red dashed line. Notably, the estimated fraction of cement coverage using monopole waveforms closely aligns with the true bond index.

[0060] The azimuthal fractions of cement coverage exhibit a smooth variation with respect to the azimuthal angle, peaking at the center of the cement channel. This smooth variation is a result of the averaging effect caused by the wavelength of acoustic logging, which ranges from approximately 1 to 2 feet, comparable to the size of the cased hole. Despite this averaging effect, the azimuthal fractions of cement coverage can still provide valuable qualitative insights into the distribution of cement around the hole.

[0061] Moving to the right panel of FIG. **9**, the cement map constructed using the azimuthal fractions of cement coverage for thirteen cases is shown. Each case is identified by the angle of cement coverage, indicated on the y-axis. To generate the image, the four measurements of azimuthal fractions of cement coverage are interpolated and displayed azimuthally. The resulting cement map enables qualitative interpretation of the distribution of cement around the hole, with the center of the cement channel located approximately at 180 degrees.

Process Flow of the Present Invention

[0062] In one embodiment of the present invention, the process flow of the present invention is summarized in FIG. **10**. For the input waveforms to be used effectively, they need to correspond to a specific depth interval where identical dual-string conditions are present. This entails having the same tubing and casing sizes, including their respective thicknesses.

[0063] In the first step, the acquired waveforms undergo processing to eliminate any potential DC offsets present in their raw waveforms. This process is straightforward due to the existence of a quiet time interval preceding the first arrival, typically the tubing extensional wave, in the waveforms. During this quiet interval, the amplitudes of the waveforms should ideally be zero. Hence, any constant and non-zero amplitudes observed are considered as DC offsets and are subsequently subtracted from the corresponding waveforms.

[0064] The primary implementation of the method is illustrated within the block marked by the yellow outline. The initial step within this block involves selecting the receiver for processing. Throughout this memo, we have chosen to utilize the first receiver waveform to exemplify the common-receiver processing for two specific reasons. Firstly, the spacing between the SATT transmitter and the first receiver is 2 feet. By selecting the first receiver, the processing results will exhibit a vertical resolution of 2 feet, aligning with the conventional CBL bond index log's vertical resolution. Secondly, the first receiver is situated closest to the transmitter, which results in fewer reverberations (i.e., bouncing back and forth) within the wellbore. Consequently, the waveforms received by the first receiver are cleaner and more readily interpretable.

[0065] After selecting the receiver, the subsequent stage in the process requires performing in-situ calibration using waveforms in the common-receiver domain. This calibration helps identify the waveforms associated with the free pipe and well-bonded conditions, utilizing the algorithm described earlier. Once the free-pipe and well-bonded waveforms are identified, the next step involves calculating the normalized amplitudes from the monopole waveforms to determine the bond index, and calculating the normalized amplitudes from the azimuthal waveforms to generate the cement map.

[0066] While the waveforms at the first receiver were used for demonstration purposes, the suggested approach can be applied to waveforms obtained from other receivers as well. The main distinction lies in the vertical resolution of the obtained results. Based on the analysis of SATT field test data, it has been observed that the computed normalized amplitudes exhibit similarity among several receivers located closest to the transmitter, even when their receiver-to-transmitter spacings differ. Hence, as outlined in the process flow, there is an opportunity to merge the outcomes from multiple receivers by calculating statistical averages and variances to generate the final presentation. FIG. **13** shows such an example.

FIELD EXAMPLES

First Field Example

[0067] In a first field example, FIG. **11** presents a collection of plots derived from the identical example shown in FIG. **8**, which aimed to illustrate the in-situ identification of free-pipe and well-bonded waveforms. The first panel exhibits the VDL of raw waveforms recorded at the first receiver, spanning a depth range of 120-270 meters. As previously mentioned, this particular depth interval involved running a 3.5-inch tubing with SATT in the 7-inch SKK CAT well.

[0068] In the second panel of FIG. **11**, we observe the collar locators, which are obtained by processing the raw waveforms from the first panel. Specifically, this display represents the VDL of residual waveforms, which are derived by subtracting the spatial-filtering output of the raw waveforms from the original waveforms. The spatial filter employed can be a running-average or median filter applied to a few neighboring depth levels.

[0069] The residual amplitudes depicted on the VDL are a result of wave reflections and mode conversions at the casing collars. These amplitudes, therefore, serve as indicators of the locations of casing collars, which are spaced approximately 10 meters apart. To aid in the identification of collar joints, a red curve representing the root-mean-square value of the residual waveforms is superimposed on the VDL.

[0070] In the third panel of FIG. **11**, we can observe the VDL of residual waveforms, which have been obtained by subtracting the estimated free-pipe waveform using the procedure described in FIG. **8**. Notably, the residual waveforms display significant amplitudes in shallower depths (e.g., 120-140 m), indicating most favorable cement bonding conditions. Conversely, the residual waveforms closer to the free-pipe conditions at the bottom (e.g., 260-265 m) exhibit very small amplitudes. This observation aligns with previous findings and serves as further confirmation of the selection of free-pipe and well-bonded waveforms.

[0071] In the fourth panel of FIG. **11**, we can observe the monopole normalized amplitude represented by the blue curve, which has been computed using Equ. (4). Additionally, the bond index log (DBI) obtained from running the Sonic Scanner [4] without tubing in the CAT well in 2006, is overlaid as the red curve. Overall, other than a slight depth shift between two, there is a high degree of agreement between the SATT normalized amplitude and the bond index. However, in the interval of 120-130 m, there appears to be a small discrepancy, which may be attributed to the eccentric positioning of the tubing within the cased hole, suggested by the red dashed circle in the raw waveform VDL displayed in the first panel.

[0072] In the fifth panel of FIG. **11**, the cement map is depicted using normalized amplitudes derived from azimuthal waveforms at the first receiver. It is important to note that only four azimuthal measurements, spaced 90 degrees apart, were available, resulting in a low-resolution display. To enhance the visualization, the cement image has been interpolated over the full 360 degrees around the borehole. Furthermore, the image has been corrected using relative bearing measurements corresponding to the rotation of SATT during its logging in the hole.

[0073] In comparison, the last panel showcases a high-resolution acoustic impedance map obtained from the Isolation Scanner [7] in a previous survey conducted without tubing in the CAT well several years earlier. Despite the significant disparity in resolution between the two images, both qualitatively exhibit good agreement by showcasing a well-bonded section at the top and a nearly free-pipe section at the bottom.

[0074] In summary, it is important to emphasize that the Sonic Scanner log and Isolation Scanner image utilized for comparison in this example were acquired without the presence of tubing inside the casing. They were chosen to illustrate that the methodology outlined in this patent memo is capable of yielding the desired results in dual-string casing scenarios.

Second Field Example

[0075] A second field example pertains to a test well (Norce U3) by Equinor in the North Sea. The SATT test was conducted within a depth interval ranging from 570 meters to 730 meters. The wellbore has a deviation of approximately 24 degrees, and it is encased with a 9⅝-inch casing. During the test, multiple SATT runs were performed, utilizing three different tubing sizes: 3.5-inch, 4.5-inch, and 5.5-inch. In this particular example, we focus on the results obtained from running SATT with the deployment of 5.5-inch tubing within the 9⅝-inch casing.

[0076] FIG. **12** presents a set of plots displayed in a similar manner as in FIG. **11**. The first panel displays the VDL of raw waveforms at the first receiver, while the second panel showcases the VDL of collar locators. Notably, in this example, the collar locations appear to be more frequent. This can be attributed to the presence of two types of collars: tubing collars and casing collars. Distinguishing between these two collar types can be achieved by examining their respective early time of occurrence. Collars that occur early in time are associated with tubing collars, while those that occur later in time are indicative of casing collars. This differentiation allows for easy identification and distinction between the two types of collars.

[0077] The third panel shows the VDL of residual waveforms after subtracting the estimated free-pipe waveform from the raw waveforms. The identified free-pipe depth interval using the procedure described in FIG. **8** is about 580-600 m, whereas the well-bonded interval is about 700-710 m. The amplitudes of residual waveforms qualitatively indicate the top portion of the hole is close to free-pipe conditions while the lower part shows favorable bonding conditions.

[0078] In the fourth panel of FIG. **12**, we present the monopole normalized amplitude by the blue curve, which has been computed using Equ. (4). Additionally, the bond index log (DBI) obtained from running the Sonic Scanner [4] without tubing in the well a couple of years earlier is overlaid as the red curve. Overall, other than a slight depth shift between two, there is a good agreement between the SATT normalized amplitude and the bond index.

[0079] However, between the depths of 610-630 m, there seems to be a discrepancy observed between the normalized amplitude and the bond index log. We suspect that this difference may be attributed to formation creeping (also known as formation squeezing) occurring outside the casing over the course of several years. Consequently, it leads to the detection of some partial bonding conditions by the normalized amplitudes. This notion is further supported by the noticeable residual amplitudes present in the 610-630 m range after subtracting the free-pipe waveform as shown in

the third panel. A similar argument can be applied to the interval between 640-690 m, where the normalized amplitudes exhibit higher values compared to the bond index measurements obtained a couple of years ago.

[0080] In the fifth panel of FIG. **12**, the cement map is depicted using normalized amplitudes derived from azimuthal waveforms at the first receiver. It is important to note that only four azimuthal measurements, spaced 90 degrees apart, were available and the cement image has been obtained by interpolating the four measurements around the hole. Furthermore, the image has been corrected using relative bearing measurements corresponding to the rotation of SATT during its logging in the hole.

[0081] The final panel presents a high-resolution acoustic impedance map obtained from the Isolation Scanner [7] in a prior survey conducted without tubing in the well a couple of years ago. Although there is a notable difference in resolution between the two images, both demonstrate good qualitative agreement by depicting a well-bonded section at the bottom and a nearly free-pipe section at the top. It is worth noting that the impact of formation creeping, such as in the 610-630 m range, is also visible on the cement map.

Third Field Example

[0082] In a third field example, FIG. **13** presents an illustrative example utilizing the SKK CAT well data depicted in FIG. **11**. The initial three panels of the Vertical Display Log (VDL) showcase waveforms obtained from the first receiver, mirroring the corresponding panels in FIG. **10**. The fourth panel demonstrates the computed normalized amplitude obtained by combining normalized amplitudes from the first to the fifth receivers. The blue curve represents the average of the five estimates, while the yellow band encompasses the range corresponding to one standard deviation of the five estimates. Notably, wider yellow bands observed in certain intervals, such as 170-190 m, potentially indicate an uneven distribution of cement around the borehole. Conversely, in zones with free pipe (e.g., 260-270 m) or well-bonded areas (e.g., 130-135 m), the yellow bands consistently narrow down and nearly disappear. The fifth panel displays the averaged cement maps derived from the five receivers. It exhibits a slightly distinct distribution compared to the cement map in the fifth panel of FIG. **11**.

[0083] Examples in the present disclosure may also be directed to a non-transitory computer-readable medium storing computer-executable instructions and executable by one or more processors of the computer via which the computer-readable medium is accessed. A computer-readable media may be any available media that may be accessed by a computer. By way of example, such computer-readable media may comprise RAM, ROM, EEPROM, CD-ROM or other optical disk storage, magnetic disk storage or other magnetic storage devices, or any other medium that may be used to carry or store desired program code in the form of instructions or data structures and that may be accessed by a computer. Disk and disc, as used herein, includes compact disc (CD), laser disc, optical disc, digital versatile disc (DVD), floppy disk and Blu-ray® disc where disks usually reproduce data magnetically, while discs reproduce data optically with lasers.

[0084] Note also that the software implemented aspects of the subject matter claimed below are usually encoded on some form of program storage medium or implemented over some type of transmission medium. The program storage medium is a non-transitory medium and may be magnetic (e.g., a floppy disk or a hard drive) or optical (e.g., a compact disk read only memory, or "CD ROM"), and may be read only or random access. Similarly, the transmission medium may be twisted wire pairs, coaxial cable, optical fiber, or some other suitable transmission medium known to the art. The claimed subject matter is not limited by these aspects of any given implementation.

[0085] The foregoing description, for purposes of explanation, used specific nomenclature to provide a thorough understanding of the disclosure. However, it will be apparent to one skilled in the art that the specific details are not required in order to practice the systems and methods described herein. The foregoing descriptions of specific examples are presented for purposes of illustration and description. They are not intended to be exhaustive of or to limit this disclosure to the precise forms described. Obviously, many modifications and variations are possible in view of the above teachings. The examples are shown and described in order to best explain the principles of this disclosure and practical applications, to thereby enable others skilled in the art to best utilize this disclosure and various examples with various modifications as are suited to the particular use contemplated. It is intended that the scope of this disclosure be defined by the claims and their equivalents below.

What is claimed is:

1. A method for cement evaluation through dual-string pipes comprising the steps of

i) acquiring waveforms data using a cement bond logging tool;

ii) processing the acquired waveforms data to eliminate one or more potential DC offsets;

iii) selecting a first receiver to further process the processed acquired waveforms data in a common-receiver domain;

iv) performing in-situ calibration using the processed acquired waveforms data from the common-receiver domain to identify free-pipe and wall-bonded waveforms;

v) calculating normalized amplitudes from monopole waveforms and azimuthal waveforms obtained from the free-pipe and wall-bonded waveforms to determine bond index and generate cement map; and

vi) calculating statistical averages and variances using the calculated normalized amplitude to generate a final presentation.

2. The method of claim **1**, wherein a second or more receivers can also be chosen for further processing of the processed acquired waveforms in a common-receiver domain followed by the remaining steps.

3. The method of claim **1**, wherein the one or more potential DC offsets is any constant and non-zero amplitudes.

4. The method of claim **1**, wherein the in-situ calibration is done using an algorithm.

5. A system for autonomous restriction navigation comprising, the system comprising:

a processor;

memory accessible to the processor;

processor-executable instructions stored in the memory and executable by the processor to instruct the system to:

i) acquire waveforms data using a cement bond logging tool;

ii) process the acquired waveforms data to eliminate one or more potential DC offsets;

iii) select a first receiver to further process the processed acquired waveforms data in a common-receiver domain;

iv) perform in-situ calibration using the processed acquired waveforms data from the common-receiver domain to identify free-pipe and wall-bonded waveforms;

v) calculate normalized amplitudes from monopole waveforms and azimuthal waveforms obtained from the free-pipe and wall-bonded waveforms to determine bond index and generate cement map; and

vi) calculate statistical averages and variances using the calculated normalized amplitude to generate a final presentation.

6. The system of claim **5**, wherein a second or more receivers can also be chosen to further process the processed acquired waveforms in a common-receiver domain followed by the remaining steps.

7. The system of claim **5**, wherein the one or more potential DC offsets is any constant and non-zero amplitudes.

8. The system of claim **5**, wherein the in-situ calibration is done using an algorithm.

* * * * *